This is a preprint, the final version is subject to change, of the American Mineralogist (MSA)
Cite as Authors (Year) Title. American Mineralogist, in press.
DOI: https://doi.org/10.2138/am-2020-7180

Revision 1

Cl-bearing Fluorcalciobritholite in high-Ti basalts from Apollo 11 and 17: Implications for volatile histories of late-stage lunar magmas.

James P. Greenwood, Kenichi Abe, Benjamin McKeeby*

Department of Earth and Environmental Sciences, Wesleyan University, Middletown, CT 06459, USA

*Now at Department of Geology and Environmental Science, University of Pittsburgh, Pittsburgh, PA 15260 USA

REVISION 1

This is a preprint, the final version is subject to change, of the American Mineralogist (MSA)
Cite as Authors (Year) Title. American Mineralogist, in press.
DOI: https://doi.org/10.2138/am-2020-7180

Revision 1

Abstract

We report the occurrence of a previously unidentified mineral in lunar samples: a Cl-,F-,REE-rich silico-phosphate identified as Cl-bearing fluorcalciobritholite. This mineral is found in late-stage crystallization assemblages of slowly cooled high-Ti basalts 10044, 10047, 75035, and 75055. It occurs as rims on fluorapatite, or as a solid-solution between fluorapatite and Cl-fluorcalciobritholite. The Cl-fluorcalciobritholite appears to be nominally anhydrous. The Cl and Fe^{2+} of the lunar Cl-fluorcalciobritholite distinguishes it from its terrestrial analogue. The textures and chemistry of the Cl-fluorcalciobritholite argue for growth during the last stages of igneous crystallization, rather than by later alteration/replacement by Cl-, REE-bearing metasomatic agents in the lunar crust. The igneous growth of this Cl-, F-bearing and OH-poor mineral after apatite in the samples we have studied suggests that the Lunar Apatite Paradox model (Boyce et al., 2014) may be inapplicable for high-Ti lunar magmas. This new volatile-bearing mineral has important potential as a geochemical tool for understanding Cl isotopes and REE chemistry of lunar samples.

This is a preprint, the final version is subject to change, of the American Mineralogist (MSA)
Cite as Authors (Year) Title. American Mineralogist, in press.
DOI: https://doi.org/10.2138/am-2020-7180

Revision 1

INTRODUCTION

In the past decade, the phosphate mineral fluorapatite has become the most important source of information about the water and D/H evolution of the Moon (Boyce et al., 2010, 2014; McCubbin et al., 2010; Greenwood et al., 2011; Barnes et al., 2013, 2014; Tartése and Anand, 2013; Tartése et al., 2014; Robinson and Taylor, 2014; Singer et al., 2017). Lunar fluorapatite also has the largest range of Cl isotope ratios of natural materials in the Solar System (Sharp et al., 2010; Boyce et al., 2015, 2018; Barnes et al., 2016) and may prove critical to understanding isotope fractionation processes that have affected lunar reservoirs, such as degassing of lunar magmas, lunar magma ocean evolution and loss of volatiles during the giant impact event that formed the Moon.

In lunar samples, the phosphate mineral merrillite is the main carrier of rare earth elements (REE); as such, determining the partitioning of REE between lunar magmas and lunar phosphates has been the subject of extensive investigation (e.g. Joliff et al., 1993 and references therein). Interestingly, the high REE contents of lunar merrillite has led some investigators to argue for lunar metasomatism (Neal and Taylor, 1991) rather than late-stage magmatic enrichment of trace elements.

Fluorbritholite is a member of the britholite group of apatite supergroup minerals, a terrestrial REE-bearing phosphate mineral with a similar structure to apatite and characterized by a significant proportion of SiO_2 and REE due to the coupled substitution: $Si^{4+}+REE^{3+}=Ca^{2+}+P^{5+}$ [Apatite: $Ca_5(PO_4)_3$ (F,Cl,OH); Britholite: (REE, Ca)$_5$(SiO_4, PO_4)$_3$ (OH,F)] (Pasero et al., 2010). Fluorcalciobritholite was approved as a mineral in 2006, and has the simplified formula $(Ca,REE)_5[(Si,P)O_4)]_3F$ (Pekov et al., 2007). It differs from fluorbritholite, $(REE,Ca)_5(SiO_4)_3F$, in having Ca>∑REE and differs from fluorapatite in having Si>P. Fluorcalciobritholite has the compositional range $Ca_{2.5}REE_{2.5}(SiO_4)_{2.5}(PO_4)_{0.5}F$ (boundary with fluorbritholite) and $Ca_{3.5}REE_{1.5}(SiO_4)_{1.5}(PO_4)_{1.5}F$ (boundary with fluorapatite) (Pekov et al., 2007). Britholite-group minerals are commonly found in alkaline rocks, and in metasomatites and pegmatites related to syenite and nepheline-syenite complexes (Pekov et al., 2007). They typically contain high abundances of U and Th, and can be metamict. They are also found in solid-solution with apatite

in a peralkaline volcanic suite of the Kenya Rift Valley (Macdonald et al., 2008) and as inclusions in magmatic zircon of the Bandelier Tuff (Wolff and Ramos, 2014).

Here we describe a previously unidentified silico-phosphate mineral in several slowly-cooled high-Ti Apollo 11 and Apollo 17 basalts, and identify it as Cl-bearing fluorcalciobritholite. The mineral contains abundant volatiles (F, Cl) and REEs, and could be an important mineral for future studies of lunar volatile evolution, petrogenesis, and metasomatism.

SAMPLES

Thin-sections of Apollo rock samples were requested from the Lunar Sample Curator and were prepared at Johnson Space Center. We studied Apollo 11 thin-sections 10044,12, 10044,633, and 10047,70 and Apollo 17 thin-sections 75055,50, 75055,51, 75055,55 and 75035,79. A sample chip of 75055 was requested from NASA and mounted with low-temperature melting point eutectic metals in the Lunar Laboratory at Wesleyan University, and then polished without the use of water or oil (75055,123b).

The four Apollo basalts that we study here are very similar to each other in petrology and mineralogy. They are all high-Ti Apollo 11 and 17 basalts, all of the low-K variety. Dymek et al. (1975) found that 10044 and 75055 are nearly identical. 75035 is from the same boulder as 75055 and is similar in both texture and chemistry (Longhi et al., 1974), except that it has the highest sulfur content of any Apollo sample (Meyer, 2010). Beatty and Albee (1978) suggested that 10044 and 10047 were so similar as to be fragments of a single larger block. Basalt 75055 is a medium- to fine-grained intergranular to subophitic ilmenite basalt (Dymek et al., 1975). It contains 33% plagioclase, 50% clinopyroxene, 12% ilmenite, 3% SiO_2, and small proportions of troilite, Fe metal, ulvöspinel, apatite, tranquilityite, and mesostasis (Dymek et al., 1975). Plagioclase forms a discontinuous, interlocking network of stubby to elongate lath-shaped crystals (~100 μm to 3500 μm in length), enclosing pyroxene and ilmenite (Dymek et al., 1975). The crystallization sequence is believed to be plagioclase slightly before ilmenite, and then coprecipitation with pyroxene (Dymek et al., 1975). The co-crystallization of these three minerals were joined by tridymite, and then mesostasis mineral crystallization, and finally solidification of K-,Si-rich glass (Dymek et al., 1975).

This is a preprint, the final version is subject to change, of the American Mineralogist (MSA)
Cite as Authors (Year) Title. American Mineralogist, in press.
DOI: https://doi.org/10.2138/am-2020-7180

METHODS

Scanning Electron Microscope (SEM)

Backscatter electron (BSE) and secondary electron (SE) images of phosphate grains in Apollo thin-sections were taken, on sections with 30 nm thick carbon coat, with the Hitachi SU5000 Field Emission Scanning Electron Microscope (FE-SEM) at Wesleyan University. It is equipped with an Apollo Octane Silicon-drift detector and EDAX Team software.

Electron microprobe microanalysis (EPMA)

Electron microprobe analyses of phosphate minerals were obtained with the Yale JEOL JXA-8530F Field Emission "Hyperprobe" which has five wavelength-dispersive spectrometers (WDS). Appropriate mineral and glass standards were used for calibration of 24 elements (F, Na, Mg, Al, Si, Sr, Fe, Mn, Y, P, S, Cl, K, Ca, Cs, La, Ce, Nd, Sm, Gd, Dy, Er, Yb, and Pr). After testing the unknown silico-phosphate for appropriate beam conditions to minimize mobility of elements during analysis of apatite (e.g. Stormer et al., 1991), an accelerating voltage of 15 KeV with a 8 nA beam current and a 1 micron spot size was used for the unknown silico-phosphate. F and Cl were analyzed first on separate spectrometers to monitor for any change in element abundances with time, but none were seen, suggesting the lunar silico-phosphate is relatively stable under the electron beam. Standards used for the analysis of F and Cl were $RbNiF_3$ and sodalite, respectively. No change in count rates were found for F and Cl during calibration acquisition for the $RbNiF_3$ and sodalite standards. We also undertook WDS mapping of fluorapatite and silico-phosphate. The WDS mapping used similar accelerating voltage and beam current, with 100 ms dwell time, and a 0.1 μm step size in a 35 μm x 65 μm area.

Micro-Raman spectroscopy

Raman spectra of fluorapatite and silico-phosphate in lunar basalt 75055 were acquired at the Stony Brook University Vibrational Spectroscopy Laboratory, using their Wi-TEC alpha300R confocal Raman microscope system. Raman excitation was with a 50 mW frequency-doubled 532 nm Nd:YAG excitation laser for collection of unpolarized Raman spectra. Point spectra were collected using a 100x objective between 0-3700 cm^{-1}, an 1800 lines/mm grating, and a 0.76 μm spot size. Initial spectral collection consisted of 180 accumulations with a 1 s acquisition time each.

RESULTS

75055,50

In a large phosphate grain in 75055,50 a region of solid-solution with silico-phosphate and fluorapatite can be seen in the BSE image in Fig. 1. This phosphate is situated at the grain boundary between two late-stage hedenbergite grains. Two of the silico-phosphate regions can be seen: 1) a bright, sharp epitaxial rim on the NW edge of the grain, and 2) a more gradational contact of apatite-fluorcalciobritholite on the S portion of the grain that appears to be part of a late-stage mineral assemblage between two grains of hedenbergite. The silico-phosphate is F-rich and contains significant Cl, as apparent in the Cl Kα WDS map in Fig. 2. The Nd Kα WDS map in Fig. 2 shows that Nd is enriched along with Cl in the britholite region of the grain.

The Cl-bearing silico-phosphate grain is in solid solution with fluorapatite in 75055,50 (Fig. 1 and 2). Electron microprobe analyses of a traverse from apatite to silico-phosphate are shown in Fig. 3, Table 1 and Table S1, and locations of EPMA analyses are shown in Fig. 1. The brightness of this phase in BSE images arises from its enrichment in the REE.

The major element zoning for CaO, P_2O_5, SiO_2, and Ce_2O_3 are shown in Fig. 3a, and are consistent with a solid-solution between fluorapatite and Cl-bearing fluorcalciobritholite. The silico-phosphate is best described as Cl-bearing fluorcalciobritholite with a composition, based on 13 anions of:

$[Ca_{2.84}(Ce_{0.81}La_{0.36}Nd_{0.19}Pr_{0.08}Y_{0.25}Sm_{0.03}Gd_{0.10}Dy_{0.03})_{\Sigma=1.86}Sr_{0.02}Fe_{0.34})]_{\Sigma=5.05}$
$[(Si_{1.77}P_{1.21})_{\Sigma=2.98}O_{12}]$ $[F_{0.62}Cl_{0.27}]_{\Sigma=0.89}$. (n=3). This is the average of three analyses of the mineral (Table 1). The fluorcalciobritholite has significant Cl, almost 1/3 of the halogen site

occupancy. The zoning between the two minerals for F and Cl is shown in Fig. 3b. The missing halogen component could be OH, as this low level of hydroxyl probably would not have been detectable with Raman. The zoning of cations per formula unit for Ca+Fe+Sr+P and Si+REE is shown in Fig. 3c. This lunar mineral also appears to have significant Fe^{2+} substituting into the Ca-REE site in this mineral, between 3-4 weight percent FeO (Table 1). Zoning of FeO and Pr_2O_3 is shown in Fig. 3d. The sharp mineral boundary between the Cl-bearing fluorcalciobritholite and the zoned region between the two minerals is at ~43 μm from the SIMS spot, and this can be seen as a break in the element zonation trends shown in Fig. 3.

Micro-Raman analysis indicate the presence of REE's in the broad luminescent peak from 1600-2400 cm^{-1} (Fig. 4). Locations of Micro-Raman analyses are shown in Fig. 1. Two distinct peaks are observed above background radiation with similar locations to those seen in the fluorbritholite data in the RRUFF database (LaFuente et al., 2015). Figure 4 shows three of these spectra obtained from the REE-rich grain. Spectral peak fitting indicates a fluorapatite spectral match to the 950 cm^{-1} peak, but the smaller but still distinct 840 cm^{-1} peak is missing (Fig. 4). Fluorbritholite from the RRUFF database matches both peaks, but the relative intensities of the lunar sample peaks are nearly equal, in contrast to the disparity between the 840 cm^{-1} and 950 cm^{-1} britholite peaks (Fig. 4). Location 75_q represents a more apatite-rich area of the grain while 75_m and 75_n are located in the REE-enriched section. We find no detectable OH/H_2O with Raman in fluorcalciobritholite, as spectral peaks at approximately 3400cm^{-1} indicative of OH and H_2O were not observed (Fig. 4). This lack of significant OH also distinguishes this lunar fluorcalciobritholite from terrestrial fluorbritholite and britholite, which are generally OH-rich.

In 75055,50, we found three other apatite-fluorcalciobritholite grains in late-stage mineral assemblages. In grain 50-2 shown in Figure 5, the apatite-fluorcalciobritholite solid-solution appears to match crystallographic planes and appears akin to sector zoning. This grain is in a late-stage mineral assemblage of hedenbergite, apatite, and K-,Si-rich mesostasis glass. This assemblage is associated with one of the other fluorcalciobritholite grains, K-Ba feldspar, FeS, all included within a large ilmenite grain.

75055,51, 75055,55, and 75055,123b

This is a preprint, the final version is subject to change, of the American Mineralogist (MSA)
Cite as Authors (Year) Title. American Mineralogist, in press.
DOI: https://doi.org/10.2138/am-2020-7180

In 75055,51 we found two other apatite-fluorcalciobritholite grains. These two grains are associated with K-Ba feldspar, fayalite, pyroxferroite, and apatite. We did not find any apatite-fluorcalciobritholite in 75055,55 or 75055,123b, though we conducted similar searches in these samples as in 75055,50 and ,51. All six grains of fluorcalciobritholite in 75055 contain detectable Cl.

75035,79

We found three apatite-fluorcalciobritholite grains in this thin-section. The fluorcalciobritholite regions were not as pure as in 75055, but EDS peaks of Si and REE correlated with BSE intensity in these grains. None of the three grains had enough fluorcalciobritholite to assess its Cl content. The grains are in typical late-stage mesostasis areas associated with apatite, silica, K-,Si-rich glass, pyroxferroite, troilite, tranquillityite, and fayalite.

10044,12 and 10044,633

We found thirteen apatite-fluorcalciobritholite grains in 10044,12 (n=4) and 10044,633 (n=9). The fluorcalciobritholite is similar in purity to that of 75055. A Cl-rich fluorcalciobritholite grain from 10044,12 is shown in Fig. 6a and EDS spectra of spots in the apatite-rich and fluorcalciobritholite-rich regions are shown in Fig. 6b. Cl can be seen in both minerals. The high Si/P and higher REE's of spot 2 are indicative of the fluorcalciobritholite. This mineral is growing in a late-stage crystallization assemblage of hedenbergite, pyroxferroite, fayalite, silica, and tranquillityite. We also found a tiny (< 1 μm) grain of a La-rich monazite in 10044,12. This monazite is located in the same late stage mineral assemblage as an apatite grain shown in Fig. 1 of Greenwood et al. (2011).

10047,70

Four grains of Cl-rich apatite-fluorcalciobritholite were found in 10047,70. The chemistry is similar to that of Cl-bearing fluorcalciobritholite in 75055,50. All four grains are

growing in typical late-stage crystallization assemblages associated with K-, Si-rich glass, apatite, pyroxferroite, fayalite, troilite, silica, and tranquillityite.

DISCUSSION

Origin of lunar Cl-fluorcalciobritholite: Late-stage crystallization or metasomatism?

On Earth, britholite-group minerals form through extreme igneous differentiation or metasomatism and are primarily found in highly differentiated alkaline pegmatites or metasomites (Pekov et al., 2007; Petrella et al., 2014), as well as in high silica rhyolites of the Bandelier Tuff (Wolff and Ramos, 2014) and peralkaline rhyolites in the Kenya Rift Valley (MacDonald et al., 2008). The lunar Cl-fluorcalciobritholite is found in late-stage melt pockets, and is always associated with other late-stage crystallization minerals (e.g. Figs. 1, 5, 6). It is also always found with apatite, appearing as bright rims on apatite in BSE images; Cl-fluorcalciobritholite was not found as discrete grains. The continuous solid-solution of the apatite and Cl-fluorcalciobritholite, Figs. 1-3 and Table S1, is indicative of igneous growth from a late-stage melt, rather than replacement and overgrowth of apatite during a REE-metasomatic event on the Moon. The apparent igneous zoning of apatite and Cl-fluorcalciobritholite shown in Fig. 5 is also best interpreted as igneous crystallization rather than replacement by later metasomatic fluids/melts.

Comparison to terrestrial britholite-group minerals

The lunar Cl-fluorcalciobritholite is distinguished from terrestrial fluorcalciobritholite in two fundamental ways: it has significant Fe^{2+} on the M site, and has significant Cl in the halogen site. Terrestrial britholite-group minerals are not reported to contain more than trace abundances of Cl (e.g. Pekov et al., 2007), suggesting that these late-stage lunar magmas contain proportions of Cl, Fe^{2+} and REE's unlike those found on Earth. The reducing nature of lunar magmas is consistent with Fe^{2+} rather than Fe^{3+} for lunar Cl-fluorcalciobritholite. Stoichiometric considerations argue that the Fe is in the ferrous rather than ferric state in the Cl-fluorcalciobritholite (e.g. Fig. 3c). Terrestrial britholite has its halogen site dominated by OH;

the lunar Cl-fluorcalciobritholite does not appear to have significant OH, as inferred both from the absence of OH vibration peaks in micro-Raman spectra (Fig. 4), and halogen site occupancy dominated by F and Cl in the electron microprobe analyses (Table 1).

The holotype specimen of fluorcalciobritholite, found in veinlets cutting a fenitized gneiss xenolith in foyaites of the Khibiny alkaline complex (Kola peninsula, Russia) has the composition: $[Ca_{2.80}(Ce_{0.93}La_{0.54}Nd_{0.26}Pr_{0.08}Y_{0.18}Sm_{0.03}Gd_{0.03}Dy_{0.020}Yb_{0.020}Er_{0.010})_{\Sigma=2.12}$ $Th_{0.04}Mn_{0.03}Sr_{0.02})]_{\Sigma=4.99}[(Si_{1.94}P_{1.06})_{\Sigma=3}O_{12}][F_{0.76}Cl_{0.01}]_{\Sigma=0.77}$. This compares favorably with the lunar Cl-fluorcalciobritholite: $[Ca_{2.84}(Ce_{0.81}La_{0.36}Nd_{0.19}Pr_{0.08}Y_{0.25}Sm_{0.03}Gd_{0.10}Dy_{0.03})_{\Sigma=1.86}$ $Sr_{0.02}Fe_{0.34})]_{\Sigma=5.05}[(Si_{1.77}P_{1.21})_{\Sigma=2.98}O_{12}][F_{0.62}Cl_{0.27}]_{\Sigma=0.89}$. The holotype fluorcalciobritholite is associated with orthoclase, nepheline, sodalite, biotite, fayalite, gadolinite-(Ce), zircon, monazite-(Ce), zirconolite, molybdenite, löllingite, and graphite. The lunar Cl-fluorcalciobritholite is associated with very different minerals (ilmenite, hedenbergite, pyroxferroite, fayalite, K-Ba feldspar, apatite, monazite, troilite, silica, and tranquillityite), further emphasizing the unearthly chemistry of lunar high-Ti basalts.

In a peralkaline volcanic suite of the Kenya Rift Valley, apatite undergoes the coupled substitution Si+REE=Ca+P, from benmoreite to trachytes to rhyolites (Macdonald et al., 2008). The zonation of total REE, Ca, P and Si is similar to that seen in Fig. 3b for the lunar apatite. The maximum britholite component of apatite of this Kenya Rift Valley rhyolite does not reach fluorcalciobritholite, and also has lower Fe^{2+} and Cl contents relative to the lunar Cl-bearing fluorcalciobritholite.

Comparison to other lunar phosphates

Apatite has long been recognized as a major carrier of phosphate in lunar rocks and soils (Keil et al., 1970; Fuchs, 1970), and an important carrier of lunar halogens (Reed et al., 1970). The importance of apatite as a carrier of water in lunar samples and other volatiles has been recognized in the past decade (Boyce et al., 2010; McCubbin et al., 2010; Greenwood et al., 2011) and has been reviewed in McCubbin et al. (2015).

Merrillite is as an important carrier of REE's in lunar samples (e.g. Joliff et al., 1993, and references therein). Descriptions and analysis of REE-enrichment in lunar merrillite has been detailed in Apollo 14 granites with similar indications of Cl and REE enrichment during

extensive igneous fractionation during crystallization (Joliff et al., 1993). The Cl-fluorcalciobritholite mineral could be an important reservoir of REEs in the Moon and needs to be considered in future petrogenetic modeling of the Moon.

Monazite has been found previously only in basalt 10047 (Lovering et al., 1974). They postulated that it could be more common, but we have only found it in 10044, and are unaware of any other reports of this mineral (Fig. S1). This suggests that monazite is a very minor carrier of REE's in lunar samples relative to merrillite.

To our knowledge, the Cl-bearing fluorcalciobritholite has not been reported previously in lunar samples. We suspect it could be present in other slowly cooled high-Ti basalts. We do not expect it will be found in low-Ti basalts, as we have not noticed it in the past decade of extensive electron beam work on lunar phosphates from low-Ti basalts. Apatite in low-Ti basalts does undergo Si and REE enrichment, but does not exhibit comparable replacement of Si for P (e.g. Greenwood et al., 2011). The high-Ti mare basalts are generally higher in REEs and incompatible trace elements than low-Ti mare basalts (Papike et al., 1998), suggesting a possible reason why this phase is present in high-Ti basalts and not in low-Ti basalts.

Implications for volatiles of late-stage high-Ti magmas

The solid-solution growth of the apatite-fluorcalciobritholite grains suggests that late-stage high-Ti magmas were becoming depleted in phosphorus while becoming enriched in Si, REE's, and Cl. This late-crystallizing, volatile-bearing mineral indicates that following the formation of apatite, the lunar magmas of high Ti-basalts were not depleted in F or Cl. This F- and Cl-enriched mineral forming after apatite suggests that the Lunar Apatite Paradox model (Boyce et al., 2014) may break down for high-Ti basalts. Alternatively, the partition coefficients of fluorcalciobritholite and late-stage lunar magmas are not known. The large change in mineral chemistry between fluorcalciobritholite and apatite due to the coupled substitution of $Si^{4+}+REE^{3+}= Ca^{2+}+P^{5+}$ could lead to partitioning differences between the two minerals and late-stage lunar magmas.

IMPLICATIONS

315 We find a silico-phosphate mineral that is in solid-solution with apatite in several Apollo
316 11 and 17 slowly-cooled basalts. Our best characterization of this mineral is that of Cl-bearing
317 fluorcalciobritholite. The textures of the mineral indicate that it formed during normal igneous
318 crystallization in high-Ti basalts, rather than as a result of secondary metasomatism or alteration
319 (e.g. Fig. 5). Interestingly, terrestrial fluorbritholite, fluorcalciobritholite, and britholite do not
320 contain significant Cl. Therefore, the Moon may represent a unique environment where REE-
321 enrichment of phosphates is accompanied by Cl halogen site occupation.
322 The Lunar Apatite Paradox (Boyce et al., 2014) postulated that high OH contents of lunar
323 apatite are due to elemental partitioning effects of very dry magmas during extreme late-stage
324 crystallization as the magmas became depleted in F due to apatite crystallization. The Cl-
325 fluorcalciobritholite shows that this magma did not become depleted in F due to apatite
326 crystallization, suggesting that the tenets of the Lunar Apatite Paradox model may be
327 inapplicable for high-Ti mare basalts. This would predict higher volatile contents for high-Ti
328 mare basalts relative to low-Ti mare basalts. Alternatively, partition coefficients of volatiles
329 between this mineral and late-stage lunar melts are not known, and could be significantly
330 different than for apatite. Future work should explore the partitioning of volatiles between
331 phosphates and late-stage lunar melts of high-Ti basalts.
332
333 **Acknowledgements**--We thank J. Eckert for assistance with EPMA, T. Glotch with assistance
334 with Micro-Raman spectroscopy, Z. Jiang and S. Karato for assistance with EBSD, Wesleyan
335 students S. Mahmood and M. Lowe, NASA Connecticut Space Grant Consortium, NASA grants
336 NNX11AB29G and NNX14AQ76G (JPG) and support of the Wesleyan Field Emission SEM by
337 NSF-MRI 1725491 (JPG).
338
339
340 **REFERENCES**
341
342 Barnes, J.J., Tartèse, R., Anand, M., McCubbin, F.M., Neal, C.R., and Franchi, I.A. (2016) Early
343 degassing of lunar urKREEP by crust-breaching impact(s). Earth and Planetary Science Letters,
344 447, 84-94.
345

Barnes, J.J., Tartèse, R., Anand, M., McCubbin, F.M., Franchi, I.A., Starkey, N.A., and Russell, S.S. (2014) The origin of water in the primitive Moon as revealed by the lunar highlands samples. Earth and Planetary Science Letters 390, 244-252.

Barnes, J.J., Franchi, I.A., Anand, M., Tartèse, R., Starkey, N.A., Koike, M., Sano, Y., and Russell, S.S. (2013) Accurate and precise measurements of the D/H ratio and hydroxyl content in lunar apatites using NanoSIMS. Chemical Geology 337, 48-55.

Beaty, D.W. and Albee, A.L. (1978) Comparative petrology and possible genetic relations among the Apollo 11 basalts. Proceedings of the 9th Lunar Planetary Science Conference 359-463.

Boyce, J.W., Kanee, S.A., McCubbin, F.M., Barnes, J.J., Bricker, H., and Treiman, A.H. (2018) Early loss, fractionation, and redistribution of chlorine in the Moon as revealed by the lunar low-Ti mare basalt suite. Earth and Planetary Science Letters, 500, 205-214.

Boyce, J.W., Treiman, A.H., Guan, Y., Ma, C., Eiler, J.M., Gross, J., Greenwood, J.P., and Stolper E.M. (2015) The chlorine isotope fingerprint of the lunar magma ocean. Science Advances 1, DOI:10.1126/sciadv.1500380.

Boyce, J.W., Tomlinson, S.M., McCubbin, F.M., Greenwood, J.P., and Treiman, A.H. (2014) The Lunar Apatite Paradox. Science 344, 400-402.

Boyce, J.W., Liu, Y., Rossman, G.R., Guan, Y., Eiler, J. M., Stolper, E.M., and Taylor, L.A. (2010) Lunar apatite with terrestrial volatile abundances. Nature 466, 466-470.

Dymek, R.F., Albee, A.L., and Chodos, A.A., 1975. Comparative mineralogy and petrology of Apollo 17 mare basalts: Samples 70215, 71055, 74255, and 75055. Proceedings of the 6th Lunar Planetary Science Conference, 49-77.

Fuchs, L.H. (1970) Fluorapatite and other accessory minerals in Apollo 11 rocks. Proceedings of the Apollo 11 Lunar Science Conference, 475-479.

Greenwood, J.P., Itoh, S., Sakamoto, N., Warren, P., Taylor, L., and Yurimoto, H. (2011) Hydrogen isotope ratios in lunar rocks indicate delivery of cometary water to the Moon. Nature Geoscience, 4, 79-82.

Jolliff, B.L., Haskin, L.A., Colson, R.O., and Wadhwa, M. (1993) Partitioning in REE-saturating minerals: Theory, experiment, and modeling of whitlockite, apatite, and evolution of lunar residual magmas. Geochimica Cosmochimica Acta 57, 4069–4094.

Keil, K., Prinz, M., and Bunch, T.E. (1970) Mineral chemistry of lunar samples. Science 167, 597-599.

Lafuente, B., Downs R.T., Yang H., and Stone N. (2015) The power of databases: the RRUFF project. In *Highlights in Mineralogical Crystallography* (Eds. T. Armbruster and R. Danisi, Berlin, W. De Gruyter) pp. 1-30.

Longhi J., Walker D., Grove T.L., Stolper E.M., and Hays J.F. (1974) The petrology of the Apollo 17 mare basalts. Proceedings of the 5th Lunar Planetary Science Conference 447-469.

Lovering, J.F., Wark, D.A., Gleadow, A.J.W., and Britten, R. (1974) Lunar monazite: A late-stage (mesostasis) phase in mare basalt. Earth and Planetary Science Letters, 21, 164-168.

Macdonald, R., Baginski, B., Belkin, H.E., Dzierzanowski, P. and Jezak, L. (2008) REE partitioning between apatite and melt in a peralkaline volcanic suite, Kenya Rift Valley. Mineralogical Magazine, 72, 1147-1161.

McCubbin, F.M., Vander Kaaden, K.E., Tartése, R., Klima, R.L., Liu, Y., Mortimer, J., Barnes, J.J., Shearer, C.K., Treiman, A.H., Lawrence, D.J., Elardo, S.M., Hurley, D.M., Boyce, J.W., and

406 Anand, M. (2015) Magmatic volatiles (H, C, N, F, S, Cl) in the lunar mantle, crust, and regolith:
407 Abundances, distributions, processes, and reservoirs. American Mineralogist 100, 1668-1707.
408
409 McCubbin, F.M., Steele, A., Hauri, E., Nekvasil, H., Yamahita, S., and Helmley R.J. (2010)
410 Nominally hydrous magmatism on the Moon. Proceedings of the National Academy of
411 Sciences 107, 11223-11228.
412
413 Meyer, C. (2010) Lunar sample compendium. Proceedings of the 41st Lunar and Planetary
414 Science Conference, Woodlands, Texas, Abstract 1016.
415
416 Neal C.R. and Taylor L.A. (1991) Evidence for metasomatism of the lunar highlands and the
417 origin of whitlockite. Geochimica Cosmochimica Acta 55, 2965-2980.
418
419 Papike, J.J., Ryder, G., and Shearer, C.K. (1998) Lunar samples. In *Planetary Materials* (ed. J. J.
420 Papike), Mineralogical Society of America, Washington, D.C., pp. 234-397.
421
422 Pasero, M. Kampf, A.R., Ferraris, C, Pekov, I.V., Rakovan, J., and White, T.J. (2010)
423 Nomenclature of the apatite supergroup minerals. European Journal of Mineralogy, 22, 163-179.
424
425 Pekov, I.V., Pasero, M., Yaskovskaya A.N., Chukanov, N.V., Pushcharovsky, D.Y., Merlino, S.,
426 Zubkova, N.V., Kononkova, N.N., Men'shikov, Y.P., and Zadov, A.E. (2007)
427 Fluorcalciobritholite, $(Ca,REE)_5[(Si,P)]O_4)_3F$, a new mineral: description and crystal chemistry.
428 European Journal of Mineralogy,19, 95-103.
429
430 Petrella, L., Williams-Jones, A.E., Goutier, J., and Walsh. J., 2014. The nature and origin of rare
431 earth element mineralization in the Misery syenitic intrusion, Northern Quebec, Canada.
432 Economic Geology, 109, 1643–1666.
433
434 Reed, G.W.Jr., Jovanovic, S., and Fuchs L.H. (1970) Trace elements and accessory minerals in
435 lunar samples. Science 167, 501-503.
436

Robinson, K.L. and Taylor, G.J. (2014) Heterogeneous distribution of water in the Moon. Nature Geoscience 7, 401-408.

Sharp, Z.D., Atudorei, V., and Durakiewicz T. (2001) A rapid method for determination of hydrogen and oxygen isotope ratios from water and minerals. Chemical Geology, 178, 197-210.

Singer, J.A., Greenwood, J.P., Itoh, S., Sakamoto, N. and Yurimoto H. (2014) Evidence for the solar wind in lunar magmas: A study of slowly cooled samples of the Apollo 12 olivine basalt suite. Geochemical Journal, 51, 95-104.

Stormer, J.C. Jr., Pierson M.L., and Tacker, R.C. (1993) Variation of F and Cl X-ray intensity due to anisotropic diffusion in apatite during electron microprobe analysis. American Mineralogist, 78, 641-648.

Tartése R. and Anand M. (2013) Late delivery of chondritic hydrogen into the lunar mantle: Insights from mare basalts. Earth and Planetary Science Letters 361, 480-486.

Tartèse R., Anand, M., McCubbin, F.M., Elardo, S.M., Shearer, C.K., and Franchi I.A. (2014) Apatite in lunar KREEP basalts: The missing link to understanding the H isotope systematics of the Moon. Geology 42, 363-366.

Wolff, J.A. and Ramos, F.C. (2014) Processes in caldera-forming high-silica rhyolite magma: Rb-Sr and Pb isotope systematics of the Otowi member of the Bandelier Tuff, Valles Caldera, New Mexico, USA. Journal of Petrology, 55, 345-375.

FIGURE CAPTIONS

Figure 1. BSE Image of apatite and Cl-fluorcalciobritholite grain in 75055,50. Shown are locations of Raman analyses (75_q, 75_m, 75_n) and microprobe analyses (112-125). A SIMS

spot can be seen in the center of the apatite grain (Ap). Two areas of Cl-fluorcalciobritholite on the NW side of the grain and in the S of the grain are labeled (Br). Hedenbergite (Hd). Microprobe traverses from the SIMS spot to the Cl-fluorcalciobritholite (analyses 125-112) are shown in Fig. 3 and Tables 1 and S1. The region of this apatite-Cl-fluorcalciobritholite grain complex below the SIMS spot is shown in Fig. 2.

Figure 2. Wavelength Dispersive Spectrometer (WDS) maps of P Kα, Ca Kα, Cl Kα, and Nd Kα abundances in the apatite-Cl-fluorcalciobritholite of Fig. 1. Chlorine abundance is correlated with that of Nd (and other REE, not shown), suggesting a greater affinity of Cl for fluorcalciobritholite vs. apatite in this example.

Figure 3. (a) Weight % oxide vs. distance (μm) from the SIMS spot shown in Fig. 1 for SiO_2 (red triangle), Ce_2O_3 (blue circle), P_2O_5 (purple triangle), and CaO (green square). Also labeled are the endmember apatite (Ap), fluorcalciobritholite (Br) and the region of solid solution. (b) Weight % halogen vs. distance (μm) for Cl and F. Cl is seen to strongly increase in the Cl-fluorcalciobritholite. (c) Cations per formula unit (assuming 8) vs. distance (μm) for Ca+Fe+Sr+P (red triangles) and Si+ΣREE (blue circle). (d) Weight % oxide vs. distance (μm) for FeO and Pr_2O_3. FeO can be seen to be enriched in the Cl-fluorcalciobritholite.

Figure 4. Raman spectra from sample 75055,50. (A) compared to RRUFF spectra of fluorbritholite (B) and fluorapatite (C). Note the broad peak from 1600-2400cm^{-1} – a result of REE luminescence. Additionally, the two peaks occur at 950 cm^{-1} and 840 cm^{-1} similar to that of fluorbritholite but with differing intensities. The sample is clearly distinct from fluorapatite. No OH or H_2O vibration peaks were seen in the 3500 cm^{-1} range.

Figure 5. BSE image of Cl-fluorcalciobritholite and apatite in 75055,50 in a late-stage crystallization assemblage of hedenbergite (Hd), apatite (Ap), Cl-fluorcalciobritholite (Br), ilmenite (Ilm) and mesostasis (Ms). Scale bar is 30 μm; each tick is 3 μm.

Figure 6. (a) BSE image of Cl-fluorcalciobritholite and apatite in 10044,12 in a late-stage crystallization assemblage of hedenbergite (Hd), fayalite (Fa), silica phase (Si), and tranquilityite

This is a preprint, the final version is subject to change, of the American Mineralogist (MSA)
Cite as Authors (Year) Title. American Mineralogist, in press.
DOI: https://doi.org/10.2138/am-2020-7180

499 (Tr). Locations of analyses 1 and 2 are shown for (b). Scale bar is 10 μm; each tick is 1 μm. (b)
500 EDS spectra of spot 1 (top) and 2 (bottom) locations shown in (a). The Si/P ratio changes from
501 the more apatite-rich portion (1) and Cl-fluorcalciobritholite region (2).
502
503
504
505
506
507
508
509

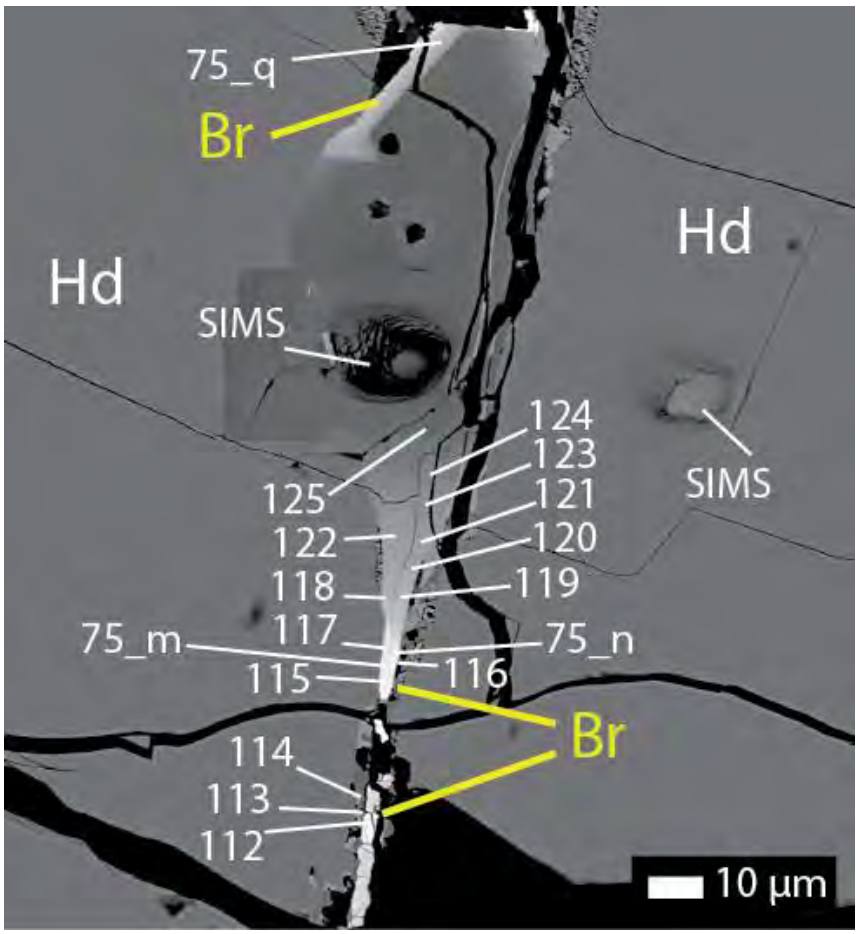

510
511
512
513 **Fig. 1.**
514

Revision 1

515

This is a preprint, the final version is subject to change, of the American Mineralogist (MSA)
Cite as Authors (Year) Title. American Mineralogist, in press.
DOI: https://doi.org/10.2138/am-2020-7180

Revision 1

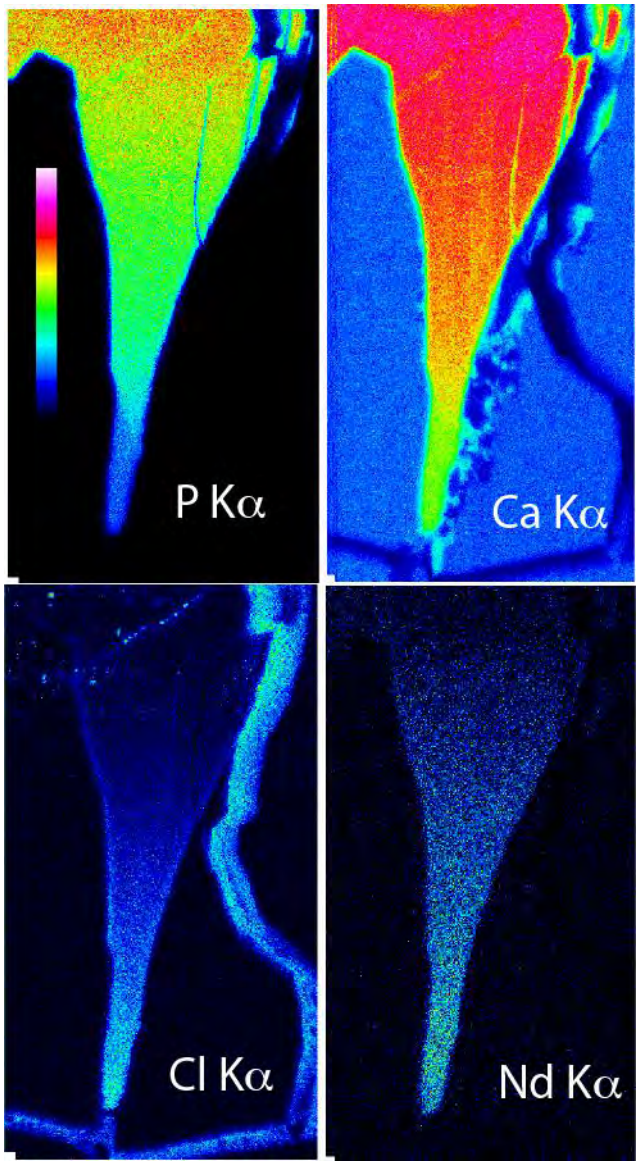

516
517
518
519
520 **Fig. 2.**

This is a preprint, the final version is subject to change, of the American Mineralogist (MSA)
Cite as Authors (Year) Title. American Mineralogist, in press.
DOI: https://doi.org/10.2138/am-2020-7180

Revision 1

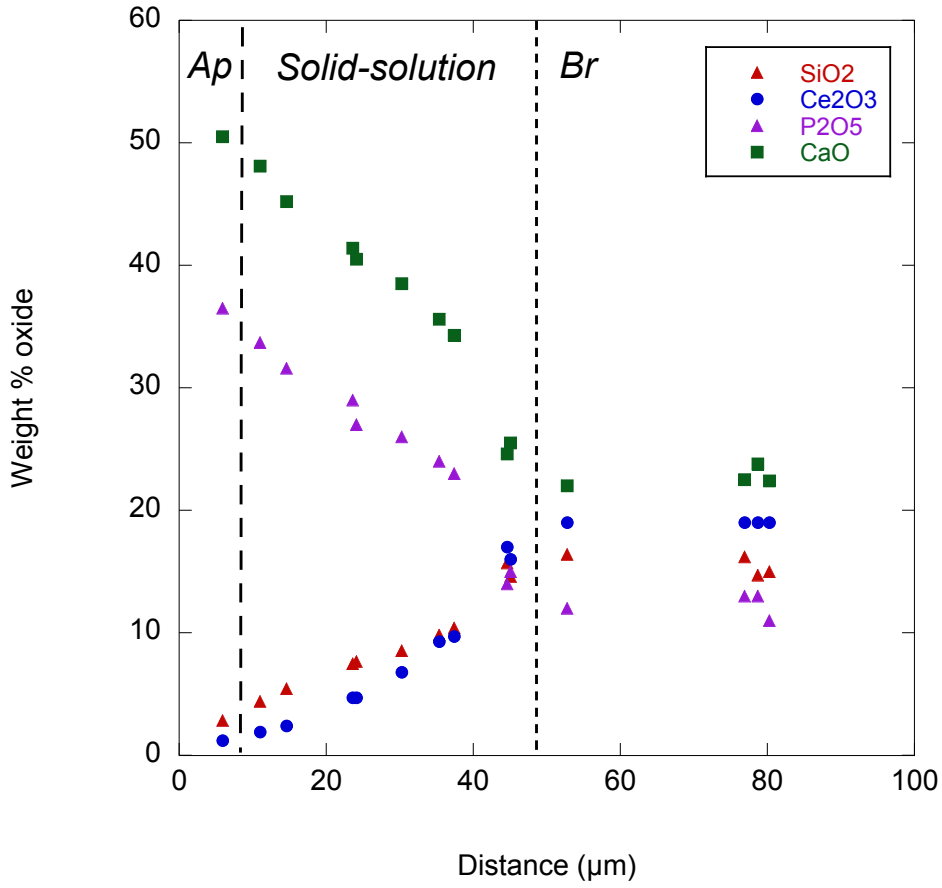

Fig. 3a.

This is a preprint, the final version is subject to change, of the American Mineralogist (MSA)
Cite as Authors (Year) Title. American Mineralogist, in press.
DOI: https://doi.org/10.2138/am-2020-7180

Revision 1

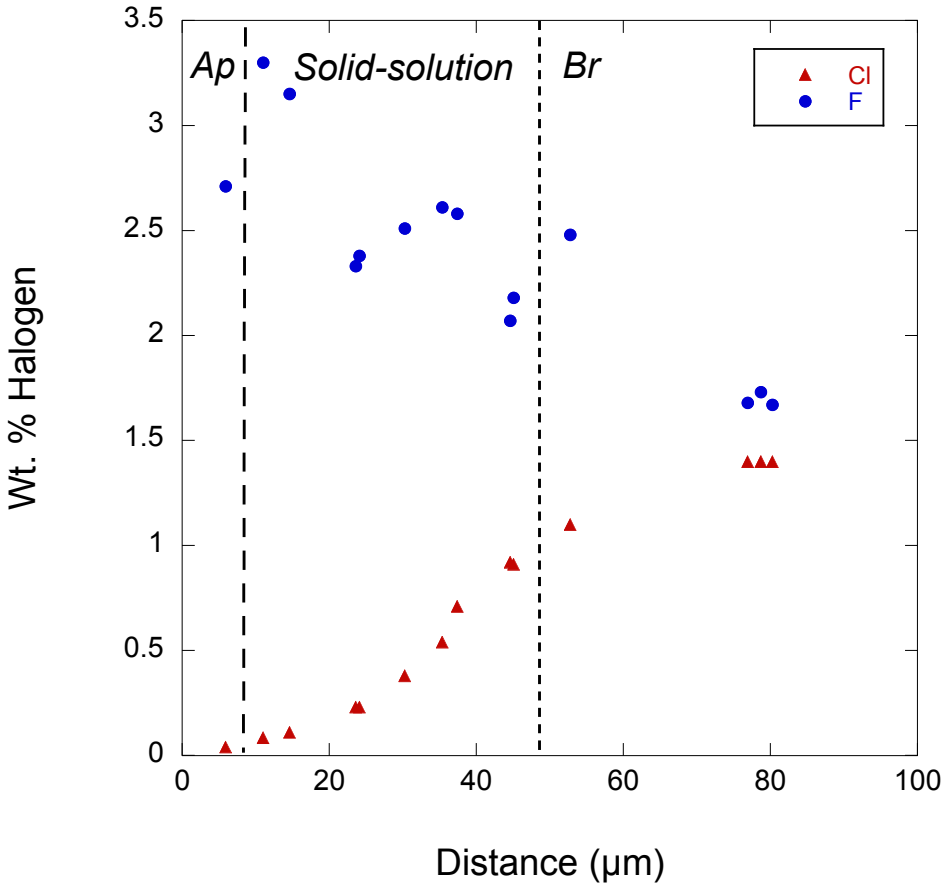

Fig. 3b.

This is a preprint, the final version is subject to change, of the American Mineralogist (MSA)
Cite as Authors (Year) Title. American Mineralogist, in press.
DOI: https://doi.org/10.2138/am-2020-7180

Revision 1

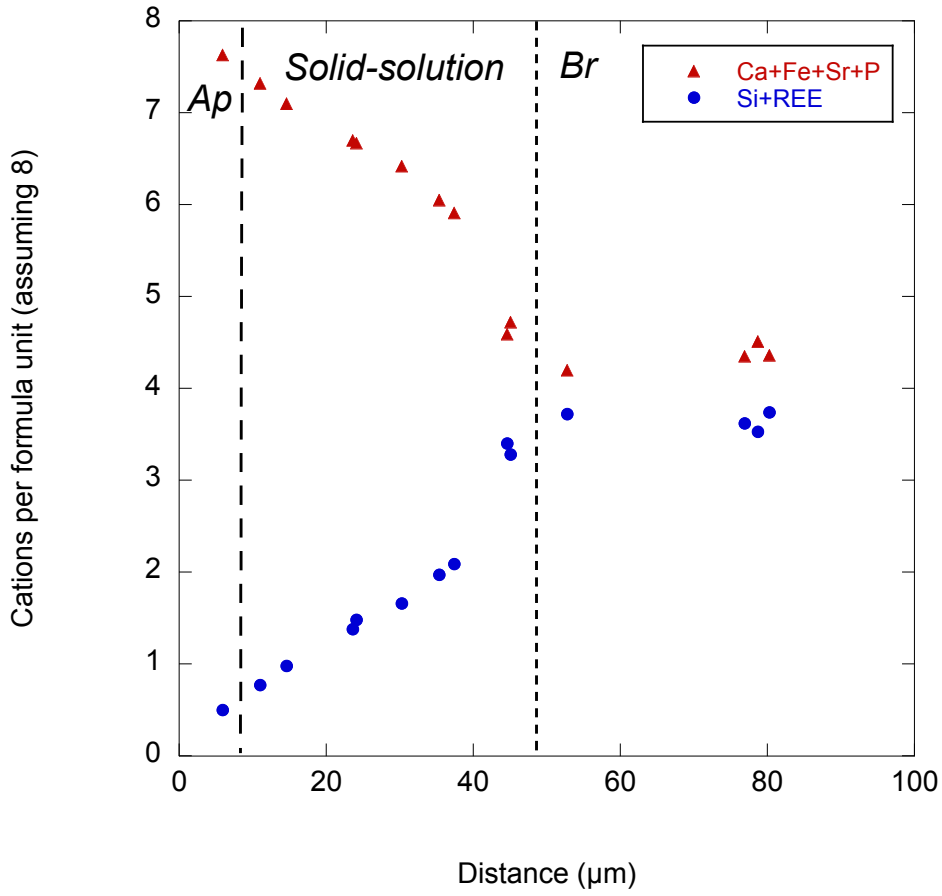

527

528

529 **Fig. 3c.**

This is a preprint, the final version is subject to change, of the American Mineralogist (MSA)
Cite as Authors (Year) Title. American Mineralogist, in press.
DOI: https://doi.org/10.2138/am-2020-7180

Revision 1

530

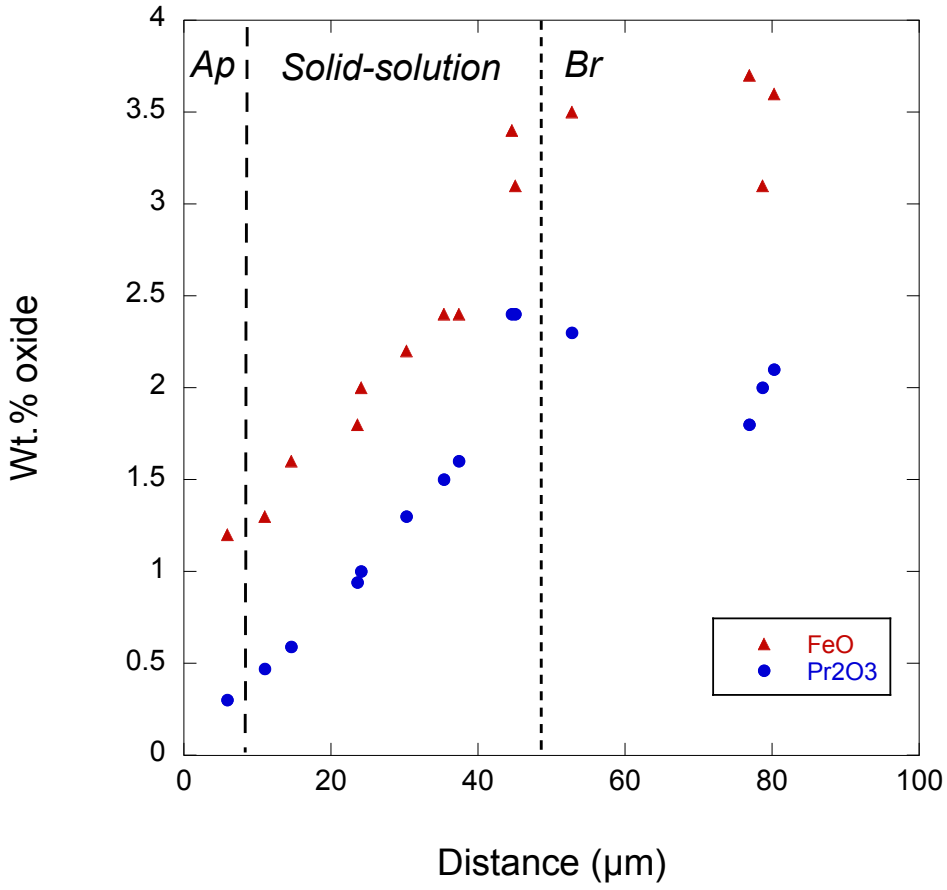

531
532 **Fig. 3d.**

This is a preprint, the final version is subject to change, of the American Mineralogist (MSA)
Cite as Authors (Year) Title. American Mineralogist, in press.
DOI: https://doi.org/10.2138/am-2020-7180

Revision 1

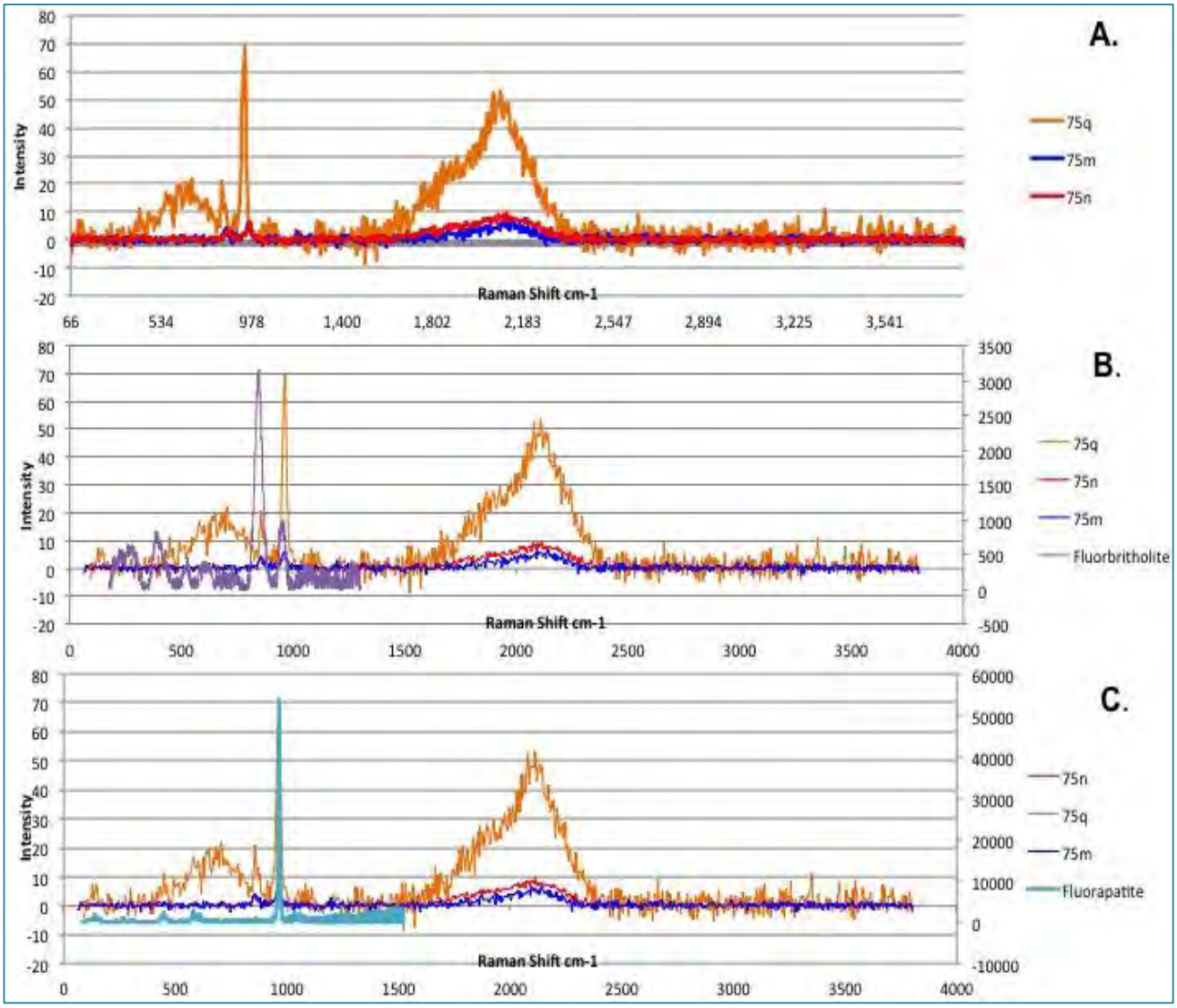

Figure 4.

This is a preprint, the final version is subject to change, of the American Mineralogist (MSA)
Cite as Authors (Year) Title. American Mineralogist, in press.
DOI: https://doi.org/10.2138/am-2020-7180

Revision 1

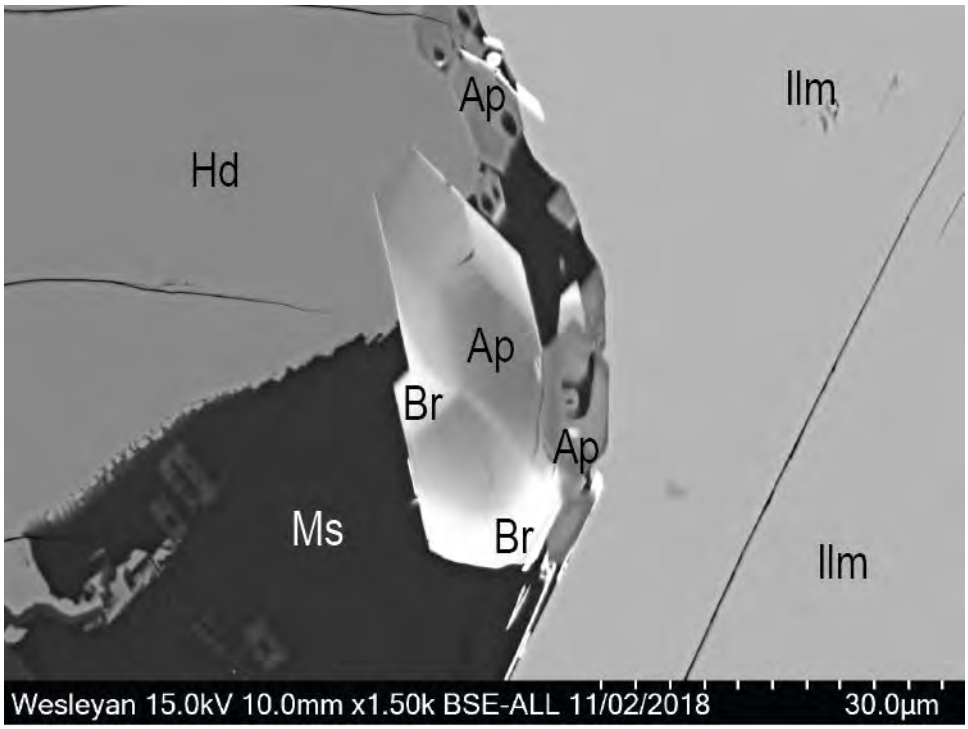

Figure 5.

This is a preprint, the final version is subject to change, of the American Mineralogist (MSA)
Cite as Authors (Year) Title. American Mineralogist, in press.
DOI: https://doi.org/10.2138/am-2020-7180

Revision 1

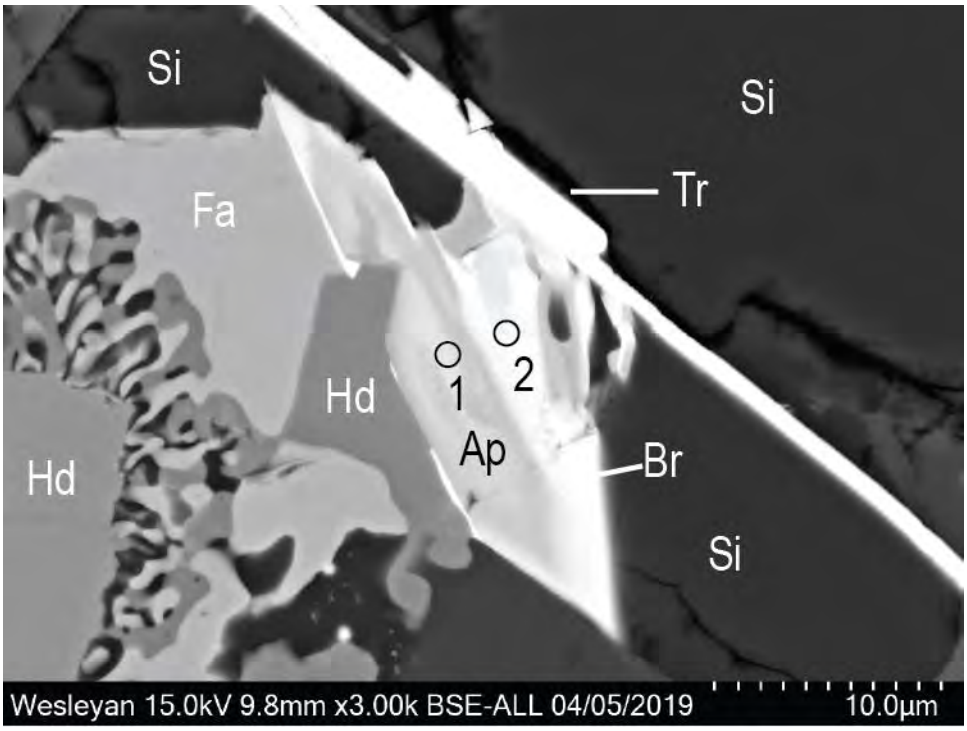

551

552

553 **Figure 6a.**

554

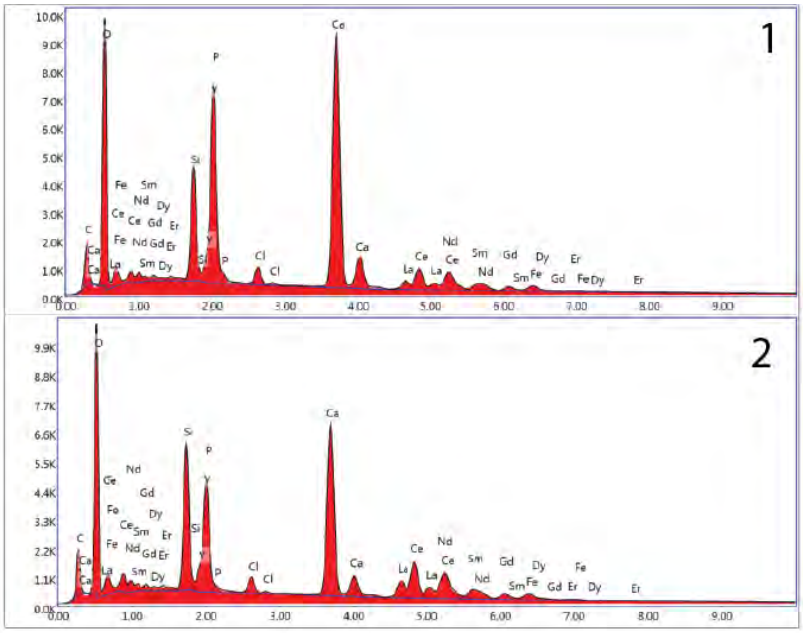

555

556 **Figure 6b.**

557

This is a preprint, the final version is subject to change, of the American Mineralogist (MSA)
Cite as Authors (Year) Title. American Mineralogist, in press.
DOI: https://doi.org/10.2138/am-2020-7180

Revision 1

Table 1: Table of elemental weight percent of elements in the Cl-fluorcalciobritholite of 75055,50 shown in Fig.1, as measured with the Yale FEG-electron microprobe. These three analyses are near 80 μm in Fig. 3. Several elements that were analyzed, but below detection limit, for these measurements were: K, Mn, Er, Yb, Al, Na and Mg.

Point#	112	113	114	Avg.
SiO_2	15	14.7	16.2	15.3
Y_2O_3	4.2	4.1	4.1	4.13
La_2O_3	9	8.3	8.3	8.53
Ce_2O_3	19	19	19	19
Pr_2O_3	2.1	2	1.8	1.97
Nd_2O_3	4.3	4.7	4.5	4.5
Sm_2O_3	0.9	0.9	0.8	0.87
Gd_2O_3	2.7	2.6	2.6	2.63
Dy_2O_3	0.7	0.8	0.7	0.73
CaO	22.4	23.8	22.5	22.9
FeO	3.6	3.1	3.7	3.47
SrO	0.3	0.3	0.3	0.3
P_2O_5	11	13	13	12.33
SO_3	1.3	0.07	0.48	0.62
Cl	1.4	1.4	1.4	1.4
F	1.67	1.73	1.68	1.69
- O = F, Cl	1.02	1.04	1.02	1.03
Total	98.55	99.46	100.04	99.35